JOURNAL OF MAGNETIC RESONANCE **130,** 119–124 (1998)
ARTICLE NO. MN971291

Optimization of Triple-Resonance HCN Experiments for Application to Larger RNA Oligonucleotides

Vladimír Sklenář,*,[1] Thorsten Dieckmann,† Samuel E. Butcher,† and Juli Feigon†,[1]

*Department of Chemistry, Faculty of Science, Masaryk University Brno, Kotlárská 2, CZ-611 37 Brno, Czech Republic; and †Department of Chemistry and Biochemistry and Molecular Biology Institute, University of California, Los Angeles, California 90095-1569

Received June 26, 1997; revised September 23, 1997

Triple-resonance NMR experiments utilizing ^{1}H, ^{13}C, and ^{15}N nuclei provide valuable information for structural studies of ^{13}C, ^{15}N-labeled oligonucleotides. Several methods for unambiguous assignment of intranucleotide connectivities between aromatic and sugar protons across the glycosidic bond have been proposed (*1–7*). These experiments correlate the ribose H1′ and base H8/6 (Hb) protons via scalar rather than dipolar interactions and therefore resolve ambiguities between the intra- and internucleotide connectivities obtained from NOE spectra. The HCN experiments (*1, 4, 5*) rely on the large proton–carbon ($^{1}J_{H,C} \sim 145–220$ Hz) and small carbon–nitrogen ($^{1}J_{C,N} \sim 7–13$ Hz) single-bond interactions in nucleotides. The relatively long evolution periods needed for efficient transfer of magnetization between the nuclei involved (70–110 ms) lower the overall sensitivity and make these experiments less useful for larger oligonucleotides with shorter T_2. In order to improve the sensitivity for applications to larger RNAs, we have revised our original 2D and 3D HCN experiments (*1*) and included several modifications.

In the original paper (*1*), two experimental schemes optimized for the H1′–{C1′}–Nb and Hb–{Cb}–Nb back and forth coherence transfers were used, and the H1′–Hb connectivities were obtained indirectly via the shared Nb glycosidic nitrogens. In the two-dimensional versions, only the chemical shift of protons and nitrogens along and adjacent to the glycosidic bond were exploited, while in the three-dimensional version additional ^{13}C labeling by the C1′ or Cb chemical shift was included. Other HCN methods (*4, 5*) also require at least two different experiments to obtain the desired correlations, and have limited sensitivity due to the long coherence transfer times needed. The approach presented here provides sugar to base correlations in a single experiment for all purine and pyrimidine nucleotides. A reduced dimensionality (*8, 9*) version of the new pulse scheme provides chemical shifts for all H1′, C1′, N9/N1, C8/C6, and H8/H6 in one two-dimensional spectrum. Additional sensitivity enhancement for all sugars and the purine bases is obtained using a multiple-quantum t_1 evolution (*10*). The performance of these experiments is demonstrated on RNA fragments of 24 and 36 nucleotides, respectively.

The modified 2D HCN experiment is shown in Fig. 1a. Although at first glance the scheme resembles the experiment proposed originally for the H8/H6–C8/C6–N1/N9 correlation in nucleotides (*1*), several significant modifications have been implemented. Since the current design follows the strategy outlined previously (*1*), only the relevant changes are discussed below. Two consecutive INEPT (*11*) and reverse INEPT steps {$^{1}H–^{13}C$} and {$^{13}C–^{15}N$} are applied to transfer the proton magnetizations H1′/Hb to their respective glycosidic nitrogens Nb and back. Band-selective ^{13}C and ^{15}N 180° pulses are applied in the {$^{13}C–^{15}N$} ''back and forth'' INEPT steps in order to achieve simultaneous correlation of H1′ and Hb protons with the glycosidic nitrogen. During the first constant time delay $2T$, the antiphase magnetizations $2H1'_z C1'_y$ and $2Hb_z Cb_y$ evolve into $4H1'_z C1'_x Nb_z$ and $4Hb_z Cb_x Nb_z$. The ^{13}C-selective 180° pulse simultaneously refocuses the C1′ and Cb transverse components while decoupling the unwanted scalar interactions (C1′–C2′ in sugars, C6–C5 and C6–C2 in pyrimidines, and C8–C4 and C8–C5 in purines). This selective excitation is accomplished using a cosinusoidal modulation (*12, 13*) ω_m superimposed on a band-selective shaped 180° pulse. Since the modulation splits the excitation spectrum into two sidebands $\omega_c \pm \omega_m$, the carbon carrier ω_c is centered between the C1′ (~88–96 ppm) and Cb (~136–142 ppm) regions, respectively, and the modulation frequency is set to $\omega_m = (\delta_{Cb} - \delta_{C1'})/2 \sim 23.5$ ppm. As a result of the off-resonance application of the shaped pulse, the transverse magnetizations of C1′ and Cb acquire the phase shift $\Delta\phi = \pm\omega_m * t_{180} * 2\pi$, where t_{180} specifies the length of the shaped pulse. To overcome the difficulties of proper phase adjustment in the subsequent INEPT step, the length t_{180} is matched to $n*1/\omega_m$, where n is an integer. The total phase shift

[1] To whom correspondence should be addressed.

1090-7807/98 $25.00

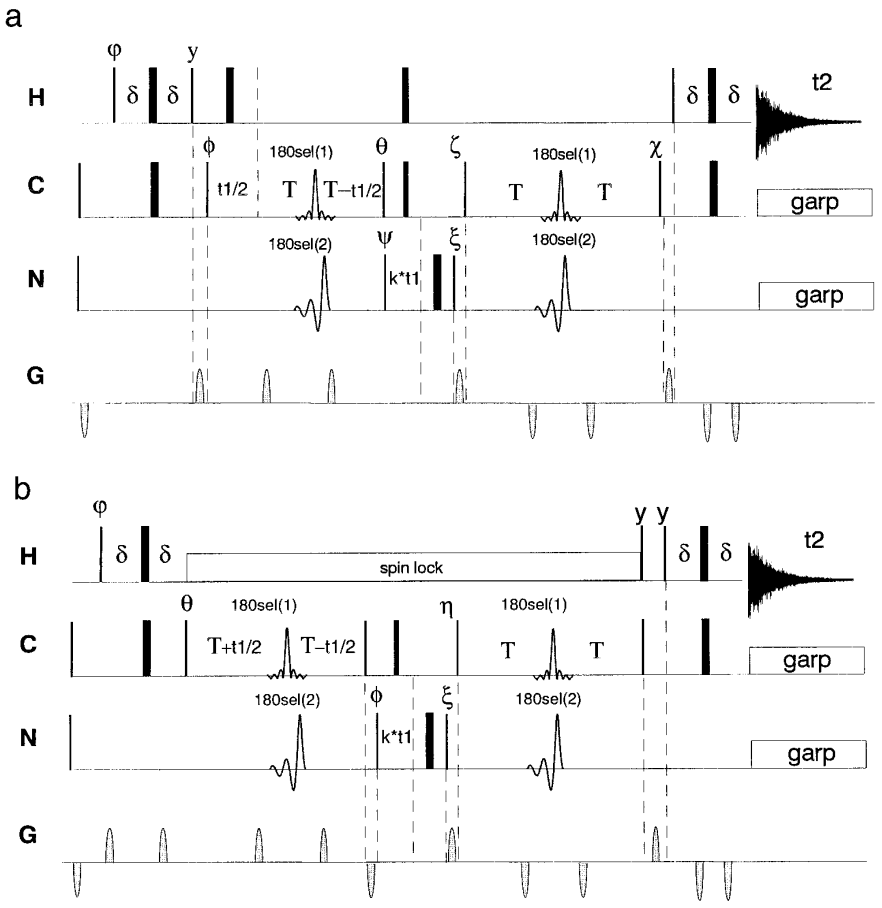

FIG. 1. Pulse schemes of the (a) single-quantum and (b) multiple-quantum 2D $^{1}H-^{13}C-\{^{15}N\}$ reduced dimensionality experiments. The thin and thick bars represent nonselective 90° and 180° pulses, respectively, applied along the x axis unless otherwise specified. The 180° pulse in the nitrogen dimension is applied to get zero chemical shift evolution for the first t_1 increment. $\delta = 1/4$, $J_{CH} \sim 1.38$ ms as a compromise for the difference between $J_{H1',C1'}$ and $J_{Hb,Cb}$, $T = 15$ ms, the 180sel(1) is a cosine-modulated REBURP (*18*) pulse, the 180sel(2) is an IBURP2 (*18*) pulse, and GARP (*21*) decoupling is applied during detection. The t_1 is incremented for ^{13}C chemical shift labeling simultaneously with $k*t_1$ to obtain cosine modulation by ^{15}N chemical shift. The phase cycling is $\varphi = x$; $\phi = x, -x$; $\theta = y, y, -y, -y$; $\psi = 4(x), 4(-x)$; $\xi(a) = 8(x), 8(-x)$; $\xi(b) = 4(x), 4(-x)$; receiver $= x, -x, -x, x, 2(-x, x, x, -x), x, -x, -x, x$; $\zeta = x$; $\chi = y$; $\eta = y$. States–TPPI phase cycling (*14*) is applied to ϕ in (a) and to θ in (b) for t_1 quadrature detection.

during the shaped pulse then becomes a multiple of 2π, and its effect can be safely neglected. The ^{15}N band-selective 180° pulse simultaneously inverts the glycosidic nitrogens N9 (purines) and N1 (pyrimidines) and is adjusted to cover the chemical shift range from 143 to 173 ppm. The purine scalar interactions C8–N7 ($J \sim 10$ Hz) are therefore successfully decoupled. In order to obtain the chemical shift of all ^{13}C and ^{15}N simultaneously, the reduced dimensionality time incrementation (*8, 9*) is applied to overcome a need for a three-dimensional experiment. States–TPPI (*14*) phase incrementation of either ϕ or ψ encodes the ^{13}C or ^{15}N chemical shifts, respectively, during the t_1 evolution. Due to the larger dispersion of the ^{13}C chemical shifts of both C1′ and Cb, it is most useful to select ^{13}C for the primary labeling and to scale the ^{15}N chemical shifts of Nb by $k*t_1$ incrementation during the ^{15}N evolution. Since the carbon carrier ω_C is centered between the C1′ and Cb regions, folding is applied to optimize the digital resolution in t_1. If the ^{13}C sweep width is set to ω_m, both the C1′ and the Cb resonances are folded once and appear in the center of the carbon dimension. Each of the H1′–C1′ and Hb–Cb peaks is split into a doublet separated by $\Delta\omega_C$ as a result of the cosinusoidal ^{15}N chemical shift modulation introduced by $k*t_1$ evolution of the $4H1'_zC1'_zNb_x$ and $4Hb_zCb_zNb_x$ antiphase magnetizations. The actual value of the Nb nitrogen chemical shift is calculated as $\delta_N = \Delta\omega_C/2*\gamma_{^{13}C}/\gamma_{^{15}N}*k$. Complete chemical shift information for all nuclei along the glycosidic bond H1′–C1′–Nb–Cb–Hb both in purines and in pyrimidines is therefore obtained from a single 2D $^{1}H-^{13}C\{^{15}N\}$ experiment. As a consequence of ^{13}C t_1 incrementation, in-phase splittings caused by the $^{13}C-^{13}C$ scalar coupling are seen in the F_1 dimension. The $^{13}C-^{13}C$ splitting is observed only at

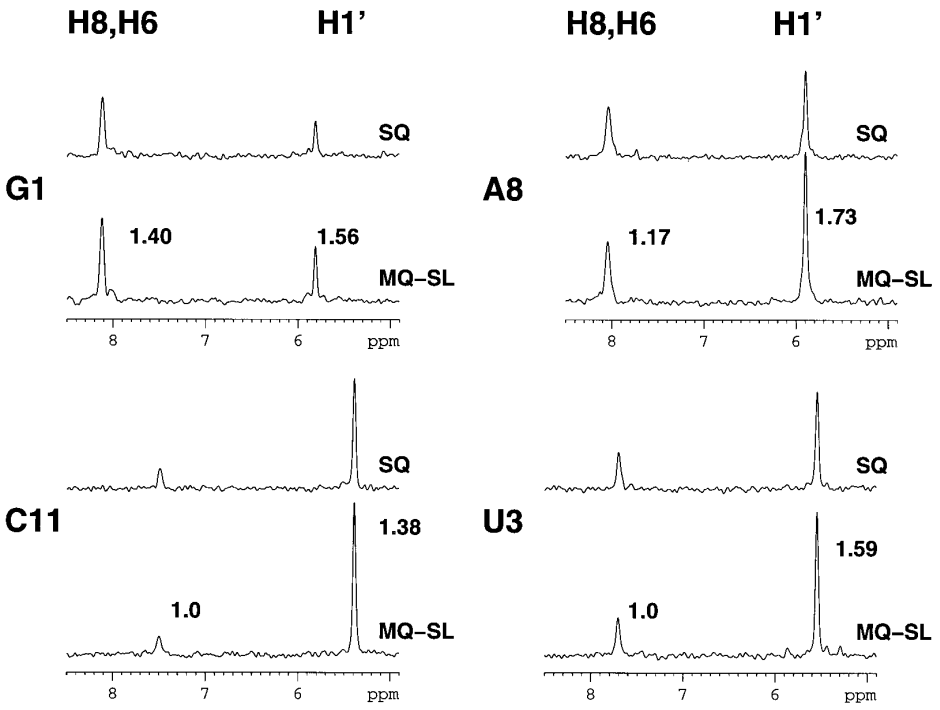

FIG. 2. Traces from 500-MHz single-quantum (SQ) and multiple-quantum spin-lock (MQ-SL) versions of the 2D $^{1}H-^{15}N$ correlation spectra of the uniformly $^{13}C,^{15}N$-labeled RNA dodecamer [r(G1G2U3G4U5G6A7A8C9A10C11C12)]$_2$ taken at the chemical shifts of G1N9, A8N9, C11N1, and U3N1. The spectra were obtained using 32 scans per t_1 increment, 512 × 96 complex points in t_2 and t_1, respectively, and a total acquisition time of 3 h to obtain a high singal-to-noise ratio for the evaluation of the enhancement factors $f_e = I_{MQ\text{-}SL}/I_{SQ}$. These factors are displayed for each pair of traces along with the signals taken from the MQ-SL experiment. The sample was 2 mM in strand in 100 mM NaCl, pH 6.0, in 450 μl at 303 K.

higher digital resolution for the relatively large C6–C5 and C1′–C2 interactions. In a simpler variant of the experiment, the 2D $^{1}H-^{15}N$ correlation of H1′ and Hb to Nb is obtained by leaving the time incrementation in the ^{15}N dimension only, with the States–TPPI phase cycling changed accordingly. In this case the $^{13}C-^{13}C$ interactions are fully decoupled during the constant time $2T$ evolution.

It has been recently demonstrated for fully $^{13}C,^{15}N$-labeled proteins that a substantial gain in sensitivity for $^{1}H-^{13}C$ correlation experiments involving the CH groups is obtained by implementing a multiple- instead of a single-quantum t_1 evolution (*10*). This is a result of the slower relaxation of the $2C_yH_x$ coherences as compared to the transverse relaxation of the antiphase proton–carbon magnetization $2C_yH_z$. In order to investigate the performance of the same approach in $^{13}C,^{15}N$-labeled RNA oligonucleotides, a multiple-quantum modification of the 2D $^{1}H-^{13}C-\{^{15}N\}$ experiment discussed above was evaluated. The pulse sequence for this experiment is outlined in Fig. 1b. The major difference from the single-quantum version is that the H1′ and Hb magnetizations are converted into multiple-quantum coherences $2H1'_xC1'_y$ and $2Hb_xCb_y$ at the end of the first $^{1}H-^{13}C$ coherence transfer. The proton–proton J modulation in the subsequent evolution is suppressed by applying a proton spin-lock field along the x axis. The carbon–nitrogen INEPT steps including modulated 180° shaped pulses and the chemical shift reduced dimensionality encoding are applied in the same way as in the single-quantum experiment. The phase-cycling scheme is modified to account for the different coherence evolution during the constant time interval $2T$, where now the proton–carbon scalar evolution is effectively decoupled.

The performance of both experiments has been tested using RNA oligonucleotides of two different sizes, a 12-base-pair (24-nucleotide) RNA duplex (*15*) and a 36-nucleotide ATP-binding aptamer complexed to AMP (*16*). To compare the sensitivity of the single-quantum (SQ) and multiple-quantum (MQ-SL) versions, two 2D $^{1}H-^{15}N$ correlation experiments were run on the uniformly $^{13}C,^{15}N$-labeled RNA dodecamer [r(GGUGUGAACACC)]$_2$ (*15*) at 500 MHz for protons. In the sample conditions used, this molecule forms a duplex with tandem G·A mismatch base pairs in the center. For both sets of experiments, a cosine-modulated REBURP (*18*) refocusing pulse with t_{180} = 4.06 ms and ω_m = 2955 Hz = 23.5 ppm at 125.76 MHz was used. The RF field strength was

increased by a factor of 2 (6 dB) with respect to a standard REBURP calibration since the excitation is split into two sidebands. The optimal setting of the constant time evolution delay $2T$ for this RNA was found experimentally to be ~36 ms. A 2.0-ms IBURP2 (*18*) pulse at 143 ppm was applied for ^{15}N z inversion. For the multiple-quantum version (*10*) of the experiment, a spin-lock field of 5.7 kHz was used with the proton carrier set to 6.9 ppm in order to sufficiently mismatch the H1′–H2′ scalar interactions. A comparison of the traces from the 2D SQ and MQ-SL spectra taken at the chemical shifts of the purine N9 and pyrimidine N1 nitrogens, respectively, for G1, A8, C11, and U3 is shown in Fig. 2. Each trace displays the correlation signals of H1′ and H8/H6 protons to their respective glycosidic nitrogens. The enhancement factors for the multiple-quantum version range from 1.0 for the pyrimidine H6/N1 to 1.73 for the sugar H1′/N9 correlation in A8. Other enhancement factors vary between 1.17 (H8/N9 in A8) and 1.59 (H1′/N1 in U3). These results clearly demonstrate that the multiple-quantum version of the experiment results in a significant gain in sensitivity for all sugar H1′/N9,N1 (38–73%) and purine H8/N9 (17–40%) correlations. In the case of the pyrimidine H6/N1 signals, no sensitivity enhancement is observed. This can be explained by interference from a Hartmann–Hahn (*19, 20*) transfer between the pyrimidine protons H6 and H5. The chemical shifts of these resonances are close to each other (H6's at 7–8 and H5's at 5.1–6.2 ppm) and have a relatively large scalar coupling (~8 Hz). The proton magnetization $H6_x$ is therefore partially converted into $2H6_yH5_z$ during the spin lock and is lost during the subsequent spin manipulations. However, careful optimization of the spin-lock field and proton carrier offset can minimize the associated loss in signal intensity.

To illustrate the high sensitivity of the experiment, the overall correlation map of the uniformly $^{13}C,^{15}N$-labeled RNA dodecamer [r(GGUGUGAACACC)]$_2$ (*15*) is shown in Fig. 3. The spectrum shown was obtained in 50 min on a 2 mM sample at 600 MHz. All H1′–N9/1 and H8/6–N9/1 correlation peaks except one are detected. The missing U5H6–U5N1 connectivity is attributed to a slow conformational exchange leading to an extensive broadening of the proton U5H6 resonance. The lower intensity of the H1′/N9 connectivities of G6 and A7 is also due to a slow conformational exchange in the U5–G6–A7 region of the RNA double helix.

The advantage of the reduced dimensionality approach for 2D $^1H-^{13}C-\{^{15}N\}$ correlation is shown in Fig. 4 using the $^{13}C,^{15}N$ G-labeled ATP binding aptamer complexed to AMP. The extensive overlap of the H1′/N9 cross peaks in the $^1H-\{^{13}C\}^{15}N$ correlation experiment (Fig. 4A) is resolved by the ^{13}C chemical shift dispersion in the 2D $^1H-^{13}C\{^{15}N\}$ spectrum (Fig. 4B). Of the 15 guanine resi-

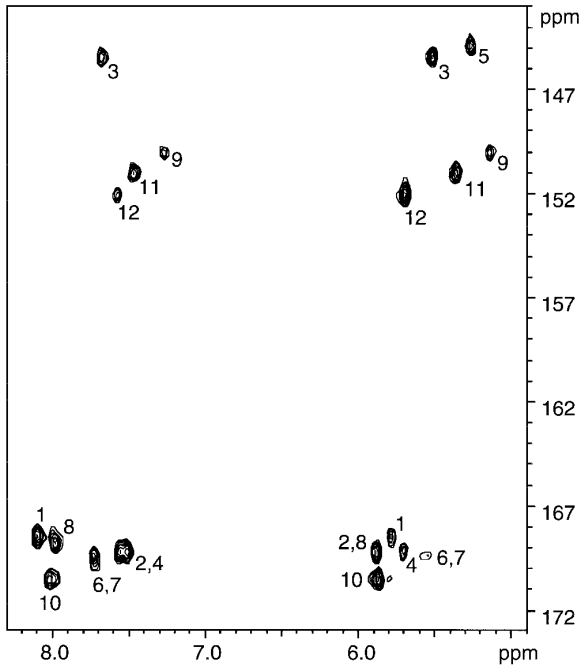

FIG. 3. Multiple-quantum two-dimensional $^1H-^{15}N$ 600-MHz spectrum of a 12-base-pair $^{13}C,^{15}N$-labeled RNA duplex [r(G1G2U3G4U5G6A7A-8C9A10C11C12)]$_2$ (*15*) at 298 K. The spectrum was acquired with spectral widths of 5 ppm in f_2 and 32 ppm in f_1, 16 scans per t_1 increment, 512 and 64 complex points in t_2 and t_1, respectively, and a total acquisition time of 50 min. The length of the REBURP pulse was 3.948 ms. The proton and carbon carriers were set to 6.9 and 114 ppm, respectively, and the spin-lock field was 6.3 kHz. The sample conditions are the same as those described in the legend to Fig. 2.

dues, only the cross peak correlating H1′/N9 from G11 is not detected since its $\delta(^{13}C) = 82.9$ ppm is shifted out of the range of other C1′ carbons. Its magnetization is therefore not refocused by the shaped 180° pulse during the constant time evolution. Thus, chemical shifts of all ^1H, ^{13}C, and ^{15}N nuclei along the glycosidic linkage were obtained on a 1.2 mM RNA sample in less than 8 h at 600 MHz.

The utility of the HCN experiment for assignment of labeled RNA molecules has been limited due to its low sensitivity in larger RNAs. The modifications of the HCN experiment presented in this paper provide a substantial gain in sensitivity and spectrometer time savings in three different ways: only one HCN spectrum is needed for both the base and the sugar correlations to the glycosidic nitrogen, additional resolution and correlations to the carbons are obtained in a two-dimensional experiment, and another factor of 1–2 in signal-to-noise ratio is gained for most resonances using the multiple-quantum t_1 evolution. Thus, this experiment should give detectable correlations for larger RNAs than has previously been possible.

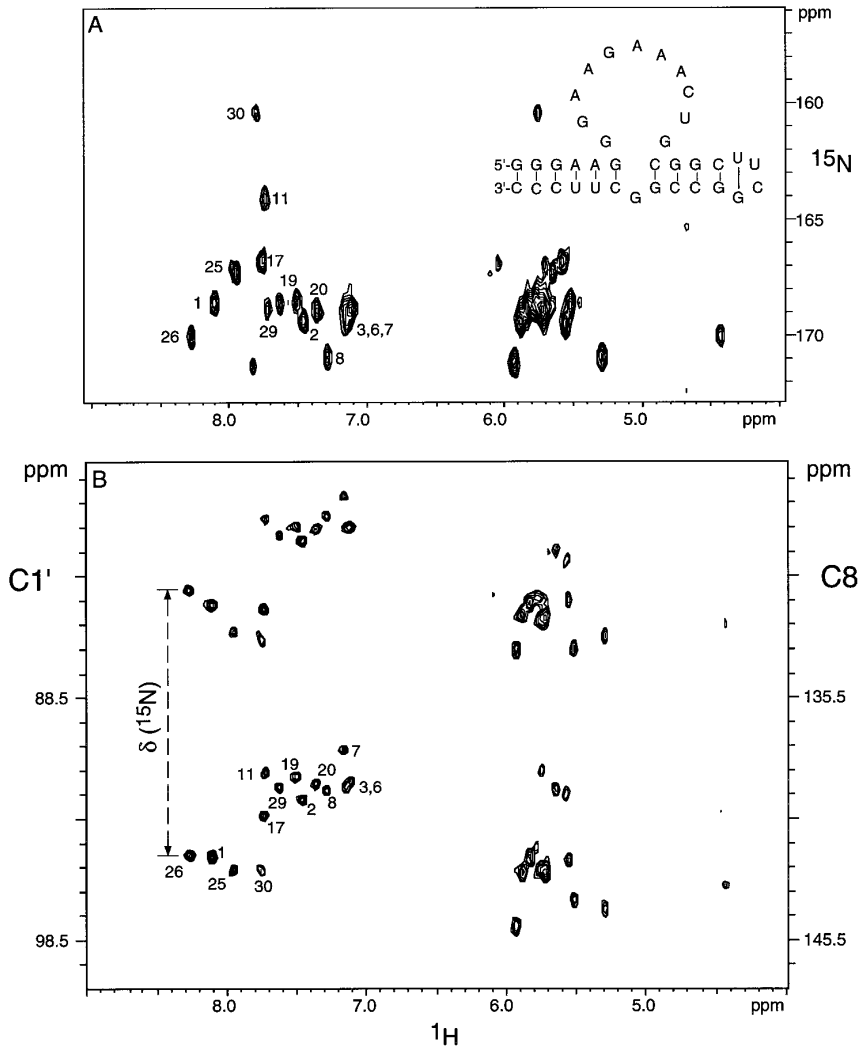

FIG. 4. 600-MHz (A) multiple-quantum two-dimensional $^{1}H-^{15}N$ and (B) reduced dimensionality multiple-quantum $^{1}H,^{13}C\{^{15}N\}$ spectra of a $^{13}C,^{15}N$-G labeled ATP-binding RNA aptamer complexed to AMP (inset) at 298 K. The spectrum in (A) was obtained using parameters analogous to those specified in the legend to Fig. 3 except that the proton carrier was set to 7.5 ppm and 32 scans per t_1 increment were acquired. The spectrum in (B) was acquired using spectral widths of 10.01 ppm in f_2 and 23.49 ppm in f_1, 128 scans per t_1 increment, 1024 and 172 complex points in t_2 and t_1, respectively, and a total acquisition time of 8 h and 35 min. The proton, carbon, and nitrogen carriers were set to 7.5, 114, and 143 ppm, respectively, and the proton spin-lock field was 7 kHz. The scaling factor used for $k*t_1$ incrementation was 2. Data were processed to give a final matrix of 2048 × 512 points using a square sine window function shifted by 75° and 90° in f_2 and f_1, respectively. The separation of the two carbon peaks correlated to one H1′/H8 corresponds to ± the N9 chemical shift (i.e., the offset from the ^{15}N carrier). This is illustrated with a dashed line for G26.

ACKNOWLEDGMENTS

This work was supported by NIH (GM 48123) and NSF (MCB-9506913) grants to J.F., the Grant Agency of the Czech Republic (203/96/1513) to V.S., and a Jane Coffin Childs postdoctoral fellowship to S.E.B.

REFERENCES

1. V. Sklenář, R. D. Peterson, M. R. Rejante, and J. Feigon, *J. Biomol. NMR* **3,** 721 (1993).
2. V. Sklenář, R. D. Peterson, M. R. Rejante, E. Wang, and J. Feigon, *J. Am. Chem. Soc.* **115,** 12181 (1993).
3. V. Sklenář, R. D. Peterson, M. R. Rejante, and J. Feigon, *J. Biomol. NMR* **4,** 117 (1994).
4. B. T. Farmer II, L. Muller, E. P. Nikonowicz, and A. Pardi, *J. Am. Chem. Soc.* **115,** 11040 (1993).
5. L. Mueller, E. P. Nikonowicz, B. T. Farmer II, and A. Pardi, *J. Biomol. NMR* **4,** 129 (1994).
6. S.-I. Tate, A. Ono, and M. Kainosho, *J. Am. Chem. Soc.* **116,** 5977 (1994).
7. V. V. Krishnamurthy, *J. Magn. Reson.* **112,** 75 (1996).
8. T. Szyperski, G. Wider, J. Bushweller, and K. Wüthrich, *J. Am. Chem. Soc.* **115,** 9307 (1993).

9. J.-P. Simorre, B. Brutscher, M. S. Caffrey, and D. Marion, *J. Biomol. NMR* **4,** 325 (1994).

10. S. Grzesiek and A. Bax, *J. Biomol. NMR* **6,** 335 (1995).

11. G. A. Morris and R. Freeman, *J. Am. Chem. Soc.* **101,** 760 (1979).

12. B. L. Tomlinson and H. D. W. Hill, *J. Chem. Phys.* **59,** 1775 (1973).

13. R. Konrat, I. Burghardt, and G. Bodenhausen, *J. Am. Chem. Soc.* **113,** 9135 (1991).

14. D. Marion, M. Ikura, R. Tschudin, and A. Bax, *J. Magn. Reson.* **85,** 393 (1989).

15. S. E. Butcher, T. Dieckmann, and J. Feigon, *J. Mol. Biol.* **268,** 348 (1997).

16. T. Dieckmann, E. Suzuki, G. K. Nakamura, and J. Feigon, *RNA* **2,** 628 (1996).

17. T. Dieckmann and J. Feigon, *J. Biomol. NMR* **9,** 259–272 (1997).

18. H. Geen and R. Freeman, *J. Magn. Reson.* **93,** 93 (1991).

19. L. Braunschweiler and R. R. Ernst, *J. Magn. Reson.* **53,** 521 (1983).

20. A. Bax and D. G. Davis, *J. Magn. Reson.* **65,** 355 (1985).

21. A. J. Shaka, P. Barker, and R. Freeman, *J. Magn. Reson.* **64,** 547 (1985).